

# A local discontinuous Galerkin method for directly solving Hamilton–Jacobi equations

Jue Yan<sup>a,\*</sup>, Stanley Osher<sup>b,2</sup>

<sup>a</sup> Department of Mathematics, Iowa State University, Ames, IA 50014, United States

<sup>b</sup> Department of Mathematics, University of California, Los Angeles, CA 90095, United States

## ARTICLE INFO

### Article history:

Received 23 February 2010

Received in revised form 3 August 2010

Accepted 20 September 2010

Available online 25 September 2010

### Keywords:

Discontinuous Galerkin method  
Hamilton–Jacobi equation

## ABSTRACT

In this paper we propose a new local discontinuous Galerkin method to directly solve Hamilton–Jacobi equations. The scheme is a natural extension of the monotone scheme. For the linear case with constant coefficients, the method is equivalent to the discontinuous Galerkin method for conservation laws. Thus, stability and error analysis are obtained under the framework of conservation laws. For both convex and nonconvex Hamiltonian, optimal  $(k+1)$ th order of accuracy for smooth solutions are obtained with piecewise  $k$ th order polynomial approximations. The scheme is numerically tested on a variety of one and two dimensional problems. The method works well to capture sharp corners (discontinuous derivatives) and have the solution converges to the viscosity solution.

© 2010 Elsevier Inc. All rights reserved.

## 1. Introduction

In this paper we develop a new discontinuous Galerkin (DG) finite element method to directly solve Hamilton–Jacobi (H–J) equations

$$\Phi_t + H(\Phi_x, \Phi_y) = 0, \quad (x, y) \in \Omega, \quad (1.1)$$

augmented with suitable initial data  $\Phi(x, y, 0) = \Phi_0(x, y)$ , and boundary conditions. Hamilton–Jacobi equations arise in many applications areas, from optimal control theory and geometrical optics, to level set methods. Examples include crystal growth, ray tracing, etching, robotic motion planning and computer vision.

Solutions to H–J equations are typically continuous but may develop singularities in the derivatives even if the initial condition is smooth. An appropriate definition of generalized solution must therefore be used, namely the viscosity solution, for which existence and uniqueness hold under suitable assumptions (see details in [11] by Crandall and Lions).

Finite difference type numerical methods for solving H–J equations have been well developed in the last two decades. In [12] Crandall and Lions first introduced a monotone numerical scheme to approximate H–J equation (1.1) and proved convergence to the viscosity solution. Later, a second order finite difference ENO scheme was developed by Osher and Sethian [20], a general framework for higher-order ENO scheme was given by Shu and Osher [21], and extension to a higher-order WENO scheme was proposed by Jiang and Peng [15]. However, on an unstructured mesh the finite difference WENO scheme [26] is complicated to implement. Also for level set applications to two-phase flow, the interface is hard to track accurately with WENO scheme [13], which in the literature is called the “mass loss” problem. All these trigger the necessity to design other good algorithms to solve H–J equations.

\* Corresponding author.

E-mail addresses: [jyan@iastate.edu](mailto:jyan@iastate.edu) (J. Yan), [sjo@math.ucla.edu](mailto:sjo@math.ucla.edu) (S. Osher).

<sup>1</sup> The research of this author is supported by NSF Grant DMS-0915247.

<sup>2</sup> This research work is supported by ONR Grant N00014-09-1-0360, UC Lab Fees Research Grant 09-LR-04-116741-BERA.

The discontinuous Galerkin method is a finite element method using a completely discontinuous piecewise polynomial space for the numerical solution and the test functions. Major development of discontinuous Galerkin methods was carried out by Cockburn, Shu and their collaborators in a series of papers [7,6,5,3,9] for nonlinear hyperbolic conservation laws. While it was being actively developed, the DG method found rapid applications in many areas, see review articles [4,10]. Discontinuous Galerkin methods become attractive and popular because: (1) it is easy to apply high order approximations, thus allowing for efficient  $p$  adaptivity; (2) it is flexible on complicated geometries, thus allowing for efficient  $h$  adaptivity; (3) it is extremely local in data communications, thus allowing for efficient parallel implementations.

For solving H–J equations with discontinuous Galerkin method, however, there are conceptual difficulties. This is because the H–J equations cannot be written in a “conservation form”, which is suitable for integration by parts, thus it is hard to define suitable numerical fluxes on the cell interfaces for discontinuous Galerkin methods. On the other hand, it is well known that H–J equations are closely related to conservation laws. In the 1D case we can claim they are equivalent. Based on this observation and the success of discontinuous Galerkin methods to conservation laws, Hu and Shu [14] developed a DG method for H–J equations in 1999. Recently in [2] Cheng and Shu proposed a new DG method directly solving H–J equations, and they focus on the convex Hamiltonians cases. Our goal is also to design a direct DG method for solving H–J equations. The DG method we use is essentially a local discontinuous Galerkin (LDG) method.

Local discontinuous Galerkin methods are designed to solve partial differential equations with higher order spatial derivatives. The idea is to introduce new variables to approximate the solution derivatives and rewrite the equation as a first order system, then apply the discontinuous Galerkin method for the system. The first LDG method was developed by Cockburn and Shu [8] for the convection diffusion equation involving second order spatial derivatives. Their work was motivated by the successful numerical experiments of Bassi and Rebay [1] for the compressible Navier–Stokes equations. Later, Yan and Shu [25] developed a LDG method for the general KdV type equation involving third order spatial derivatives. Recently LDG methods have been rapidly developed for a large number of nonlinear problems, e.g. [16,18,24].

The procedure of applying LDG method to solve H–J equations is the following. First, we introduce four new variables  $p_1$ ,  $p_2$  and  $q_1$ ,  $q_2$  to respectively approximate  $\Phi_x$  and  $\Phi_y$

$$\begin{cases} p_1 - \Phi_x = 0, \\ p_2 - \Phi_x = 0, \end{cases} \quad \begin{cases} q_1 - \Phi_y = 0, \\ q_2 - \Phi_y = 0. \end{cases}$$

This is carried out by solving the standard upwind discontinuous Galerkin method, namely  $p_1$  and  $p_2$  are auxiliary variables used to approximate  $\Phi_x$  with numerical flux chosen from the right ( $\Phi_x^+$ ) and the left ( $\Phi_x^-$ ), respectively, and  $q_1$  and  $q_2$  are used to approximate  $\Phi_y^+$  and  $\Phi_y^-$  correspondingly. We see  $p_1$  is nearly identical to  $p_2$  when the solution is smooth, but at corners  $p_1$  and  $p_2$  are totally different. Thus  $p_1$  and  $p_2$  together can fully capture the characteristic of  $\Phi_x$  when the solution have discontinuous derivatives. Similarly, this mechanism guarantees  $q_1$  and  $q_2$  can capture complete information of  $\Phi_y$ . Then we plug them into a monotone consistent numerical Hamiltonian  $\hat{H}(p_1, p_2, q_1, q_2)$  and solve the H–J equation in the weak sense. For piecewise constant approximations, our scheme degenerates to the standard monotone scheme, which guarantees its convergence to the viscosity solution. In some sense, we can claim our scheme is a natural extension of the monotone scheme within DG framework. We should mention that none of the other DG methods [14,2,17] works with piecewise constant approximations.

For the linear constant coefficient case, the method is equivalent to the discontinuous Galerkin method for conservation laws. Thus, stability and error analysis are carried out in the same way as for conservation laws. For the linear variable coefficient problem, our scheme is not exactly the same as the standard discontinuous Galerkin method, but the LDG scheme captures the characteristics correctly and numerically we obtain optimal order of accuracy with smooth variable coefficients. We test the LDG methods on a variety of one and two dimensional Hamilton–Jacobi equations. For both convex and nonconvex Hamiltonian, optimal  $(k + 1)$ th order of accuracy for smooth solutions are obtained with piecewise  $k$ th degree polynomial approximations. The method works well to capture sharp corners (discontinuous derivatives) and the LDG solution converges to the viscosity solution.

In this paper we use capital letters  $\Phi$  etc. to denote the exact solutions to the H–J equations and lower case letters  $\phi$  to denote the discontinuous Galerkin numerical solutions. This paper is organized as follows: In Section 2, we introduce the formulation of local discontinuous Galerkin method for the one-dimensional H–J equations. The generalization of LDG methods to two-dimensional H–J equations is discussed in Section 3. In Section 4, we present a series of numerical results to validate the LDG methods.

## 2. The LDG scheme formulation and theoretical results for the one dimensional case

In this section we define our LDG method for solving Hamilton–Jacobi equation (1.1) in one-dimensional setting

$$\Phi_t + H(\Phi_x) = 0, \quad x \in \Omega. \tag{2.2}$$

First let’s introduce some notations. The computational mesh is given by  $\Omega = \{I_j = (x_{j-\frac{1}{2}}, x_{j+\frac{1}{2}}), j = 1, \dots, N\}$ . We denote  $x_j = \frac{1}{2}(x_{j-\frac{1}{2}} + x_{j+\frac{1}{2}})$  as the center of the cell  $I_j$  and  $\Delta x_j = x_{j+\frac{1}{2}} - x_{j-\frac{1}{2}}$  as the size of each cell. We denote  $\Delta x = \max_j \Delta x_j$ . The numerical solution space  $\mathcal{V}_{\Delta x}$  is defined as the piecewise polynomial space where there is no continuity requirement at the cell interface  $x_{j\pm 1/2}$ .

$$\mathcal{V}_{\Delta x} = \left\{ v \in L^2(\Omega) : v|_{I_j} \in P^k(I_j), j = 1, \dots, N \right\}, \tag{2.3}$$

where  $P^k(I_j)$  denotes the polynomial space on  $I_j$  with degree at most  $k$ .

The local discontinuous Galerkin method is defined as the following: We seek a numerical solution  $\phi \in \mathcal{V}_{\Delta x}$  such that for all test function  $u \in \mathcal{V}_{\Delta x}$  we have

$$\int_{I_j} \phi_t u \, dx + \int_{I_j} \widehat{H}(p_1, p_2) u \, dx = 0, \quad \forall j = 1, \dots, N, \tag{2.4}$$

where  $p_1$  and  $p_2$  are two new variables we introduce to approximate  $\Phi_x$ , and  $\widehat{H}(p_1, p_2)$  is the monotone consistent numerical Hamiltonian we choose to approximate  $H(\Phi_x)$ .

Just as those defined in the LDG method [8],  $p_1$  and  $p_2$  are two auxiliary variables. Both  $p_1$  and  $p_2$  are introduced to approximate  $\Phi_x$ . Here  $p_1$  is to approximate  $\Phi_x$  with numerical flux chosen from the right (upwind right), like  $\phi_x^+$  in [15]. In a word, for any test function  $v \in \mathcal{V}_{\Delta x}$ ,  $p_1 \in \mathcal{V}_{\Delta x}$  is obtained by solving the following right upwind DG scheme

$$\int_{I_j} p_1 v \, dx + \int_{I_j} \phi v_x \, dx - \phi_{j+1/2}^+ v_{j+1/2}^- + \phi_{j-1/2}^+ v_{j-1/2}^+ = 0. \tag{2.5}$$

Here the following notations have been used:

$$\phi^\pm = \phi(x \pm 0, t).$$

Variable  $p_2$  is introduced to approximate  $\Phi_x$  with the numerical flux chosen from the left (upwind left). For any test function  $w \in \mathcal{V}_{\Delta x}$ ,  $p_2 \in \mathcal{V}_{\Delta x}$  is obtained through the following left upwind DG scheme

$$\int_{I_j} p_2 w \, dx + \int_{I_j} \phi w_x \, dx - \phi_{j+1/2}^- w_{j+1/2}^- + \phi_{j-1/2}^- w_{j-1/2}^+ = 0. \tag{2.6}$$

Finally we replace  $H(\Phi_x)$  in Eq. (2.2) by a monotone consistent numerical Hamiltonian  $\widehat{H}(p_1, p_2)$ , for monotone we mean  $\widehat{H}(1, \uparrow)$  that is a none increasing function for the first argument and a none decreasing function for the second argument. For consistency we mean  $\widehat{H}(p, p) = H(p)$ . At each time step, we first locally compute  $p_1$  and  $p_2$  from (2.5) and (2.6), then plug  $p_1$  and  $p_2$  into the numerical Hamiltonian  $\widehat{H}(p_1, p_2)$ , multiply it with any test function  $u \in \mathcal{V}_{\Delta x}$ , integrate over cell  $I_j$  and update  $\phi$  to the next time level. This completes the definition of the LDG scheme. For time discretization, we use explicit third-order TVD Runge–Kutta method as in [22].

In this paper, we simply use the Lax–Friedrichs numerical Hamiltonian

$$\widehat{H}(p_1, p_2) = H\left(\frac{p_1 + p_2}{2}\right) - \frac{1}{2}\alpha(p_1 - p_2)$$

with  $\alpha = \max_{p \in D} \left| \frac{\partial H(p)}{\partial p} \right|$ . With  $D$  taken as a local domain, namely  $D$  is evaluated locally as  $D = [\min(p_1, p_2), \max(p_1, p_2)]|_{I_j}$  we call it a local Lax–Friedrichs scheme. With  $D$  taken as a global domain, namely  $D$  is evaluated over the whole computational domain and defined as  $D = [\min(p_1, p_2), \max(p_1, p_2)]|_{\Omega}$  we call it the global Lax–Friedrichs scheme. We should comment that numerical experiments show that there is little difference between the global and the local Lax–Friedrichs schemes.

With piecewise constant approximations, we see the LDG scheme degenerates to a monotone scheme. We know even monotone scheme is only first order, it guarantees its convergence to the viscosity solution. Let’s use the notation  $\phi_j^n$  to represent the constant approximation for the solution  $\Phi$  in cell  $I_j$  at time  $t = t_n$ , and use  $\Delta x$  as the uniform partition step size in space and  $\Delta t$  in time. From (2.5) and (2.6), we see  $p_1$  and  $p_2$  become the forward and backward approximation to  $\Phi_x$  as

$$(p_1)_j^n = \frac{\phi_{j+1}^n - \phi_j^n}{\Delta x}, \quad (p_2)_j^n = \frac{\phi_j^n - \phi_{j-1}^n}{\Delta x}.$$

Plug them into (2.4) and use the Euler forward discretization in time, we have

$$\phi_j^{n+1} = \phi_j^n - \Delta t \left\{ H\left(\frac{\phi_{j+1}^n - \phi_{j-1}^n}{2\Delta x}\right) - \frac{\alpha}{2} \left(\frac{\phi_{j+1}^n - 2\phi_j^n + \phi_{j-1}^n}{\Delta x}\right) \right\} = G(\phi_{j-1}^n, \phi_j^n, \phi_{j+1}^n).$$

With suitable Lax–Friedrichs coefficient  $\alpha$ , we can easily have  $G$  as a monotone increasing function in its three arguments. Thus we claim the LDG method is a natural extension of the monotone scheme under the discontinuous Galerkin method framework.

Now we turn to the question of the quality of the numerical solution defined by the LDG method. If the Hamiltonian  $H(\Phi_x)$  is a linear function, Eq. (2.2) degenerates to a linear wave equation (2.7), for simplicity we assume  $a > 0$  is a constant

$$\Phi_t + a\Phi_x = 0. \tag{2.7}$$

Now the numerical Hamiltonian  $\widehat{H}(p_1, p_2)$  degenerates to a simple upwind flux  $ap_2$ , and LDG scheme (2.4)–(2.6) is simplified as follows:

$$\begin{cases} \int_{I_j} \phi_t u dx + \int_{I_j} a p_2 u dx = 0, \\ \int_{I_j} p_2 w dx + \int_{I_j} \phi w_x dx - \phi_{j+1/2}^- w_{j+1/2}^- + \phi_{j-1/2}^- w_{j-1/2}^+ = 0. \end{cases} \tag{2.8}$$

It's easy to see, with the same test function  $u = w$ , the LDG scheme (2.8) is nothing but a standard upwind DG scheme. So we have the following optimal error estimate for the linear problem (2.7).

**Proposition 2.1** (Error estimate). *Suppose the exact solution  $\Phi$  of (2.7) is smooth and numerical solution  $\phi$  is obtained with our scheme (2.8). Let  $e(\cdot, t)$  be the approximation error  $\Phi - \phi$ . Then we have*

$$\|e(\cdot, T)\|_{L^2(\Omega)} \leq C |\Phi_0|^{k+2} (\Delta x)^{k+1}, \tag{2.9}$$

where  $C$  depends on  $k, a$  and the final time  $T$ .

For variable coefficient linear Hamilton–Jacobi equation

$$\Phi_t + a(x)\Phi_x = 0, \tag{2.10}$$

the scheme (2.4) becomes

$$\int_{I_j} \phi_t u dx + \int_{I_j} \left\{ \frac{p_1}{2} (a(x) - \max_{I_j} |a(x)|) u + \frac{p_2}{2} (a(x) + \max_{I_j} |a(x)|) u \right\} dx = 0. \tag{2.11}$$

Note that even the scheme (2.11) is not exactly the same as the standard DG method for (2.10), however the scheme catches the upwind directions correctly. Numerically we obtain optimal  $(k + 1)$ th order of accuracy for  $p^k$  polynomial approximations with smooth variable coefficient  $a(x)$ .

### 3. The LDG scheme formulation for the two dimensional case

In this section, we generalize the LDG scheme discussed in the previous section to the two spatial dimensions. The algorithm in more spatial dimensions is similar. For 2D, the scalar HJ equation is

$$\Phi_t + H(\Phi_x, \Phi_y) = 0, \quad (x, y) \in \Omega[0, 1] \times [0, 1] \tag{3.12}$$

with suitable initial condition  $\Phi(x, y, 0) = \Phi_0(x, y)$  and boundary conditions. Notice that the assumption of a unit box geometry and periodic boundary conditions is for simplicity only and is not essential: the method can be easily designed for arbitrary domain and for non-periodic boundary conditions.

Let's denote a triangulation of the unit box by  $T_{\Delta x} = \{K\}$ , consisting of non-overlapping triangles covering completely the unit box. We assume the triangles  $K$  to be shape-regular. Here  $\Delta x = \text{diam}\{K\}$  measures the diameter of the triangle  $K$ . We again denote the finite element space by

$$\mathcal{V}_{\Delta x} = \left\{ v \in L^2(\Omega) : v|_K \in P^k(K), \forall K \in T_{\Delta x} \right\}, \tag{3.13}$$

where  $P^k(K)$  is the set of all polynomials of degree at most  $k$  on cell  $K$ . We propose a discontinuous Galerkin method for (3.12) as follows: we seek  $\phi \in \mathcal{V}_{\Delta x}$  such that for all test function  $u \in \mathcal{V}_{\Delta x}$  and all cells  $K \in T_{\Delta x}$  we have

$$\int_K \phi_t u dx dy + \int_K \widehat{H}(p_1, p_2, q_1, q_2) u dx dy = 0. \tag{3.14}$$

Here again  $\widehat{H}(p_1, p_2, q_1, q_2)$  is a monotone consistent numerical Hamiltonian we choose to approximate  $H(\Phi_x, \Phi_y)$ . Four new auxiliary variables  $p_1, p_2$  and  $q_1, q_2$  are introduced to approximate  $\Phi_x$  and  $\Phi_y$ , respectively.

Variables  $p_1$  and  $p_2$  are both used to approximate  $\Phi_x$ . Similar to the 1D case, we obtain  $p_1$  and  $p_2$  by solving two simple upwind DG schemes. We seek  $p_1 \in \mathcal{V}_{\Delta x}$  and  $p_2 \in \mathcal{V}_{\Delta x}$  such that for any test functions  $v_1 \in \mathcal{V}_{\Delta x}$  and  $v_2 \in \mathcal{V}_{\Delta x}$  we have

$$\begin{cases} \int_K p_1 v_1 dx dy + \int_K \phi(v_1)_x dx dy - \int_{\partial K} \phi^+ n_x v_1^{int_K} ds = 0, \\ \int_K p_2 v_2 dx dy + \int_K \phi(v_2)_x dx dy - \int_{\partial K} \phi^- n_x v_2^{int_K} ds = 0 \end{cases} \tag{3.15}$$

with

$$\phi^+ = \begin{cases} \phi^{ext_K}, & \text{if } n_x \geq 0, \\ \phi^{int_K}, & \text{else} \end{cases}$$

and

$$\phi^- = \begin{cases} \phi^{int_K}, & \text{if } n_x \geq 0, \\ \phi^{ext_K}, & \text{else,} \end{cases}$$

where  $\partial K$  is the boundary of element  $K$ ,  $n = (n_x, n_y)$  is the outward unit normal for element  $K$  along the element boundary  $\partial K$ . Here we use  $\phi^{int_K}$  to denote the value of  $\phi$  on  $\partial K$  evaluated from inside the element  $K$ . Correspondingly we use  $\phi^{ext_K}$  to denote

the value of  $\phi$  on  $\partial K$  evaluated from the outside element  $K$  (inside the neighboring element  $K'$  which shares the same edge with  $K$ ).

The two new variables  $q_1$  and  $q_2$  are used to approximate  $\Phi_y$  and obtained by solving the following two upwind DG schemes. We seek  $q_1 \in \mathcal{V}_{\Delta_x}$  and  $q_2 \in \mathcal{V}_{\Delta_x}$  such that for any test functions  $w_1 \in \mathcal{V}_{\Delta_x}$  and  $w_2 \in \mathcal{V}_{\Delta_x}$  we have

$$\begin{cases} \int_K q_1 w_1 dx dy + \int_K \phi(w_1)_y dx dy - \int_{\partial K} \phi^+ n_y w_1^{int_K} ds = 0, \\ \int_K q_2 w_2 dx dy + \int_K \phi(w_2)_y dx dy - \int_{\partial K} \phi^- n_y w_2^{int_K} ds = 0 \end{cases} \tag{3.16}$$

with

$$\phi^+ = \begin{cases} \phi^{ext_K}, & \text{if } n_y \geq 0, \\ \phi^{int_K}, & \text{else} \end{cases}$$

and

$$\phi^- = \begin{cases} \phi^{int_K}, & \text{if } n_y \geq 0, \\ \phi^{ext_K}, & \text{else.} \end{cases}$$

Finally, to complete the definition of LDG scheme, we choose a monotone consistent numerical Hamiltonian  $\hat{H}(p_1, p_2, q_1, q_2)$ , for monotone we mean  $\hat{H}(\downarrow, \uparrow, \downarrow, \uparrow)$  and for consistency we mean  $\hat{H}(p, p, q, q) = H(p, q)$ . Then plug  $p_1, p_2$ , computed from (3.15) and  $q_1, q_2$  computed from (3.16), into the numerical Hamiltonian  $\hat{H}(p_1, p_2, q_1, q_2)$ , multiply it with any test function  $u \in \mathcal{V}_{\Delta_x}$  and integrate over the element  $K$  and update  $\phi(x, y, t)$  to the next time level.

Here we simply use the Lax–Friedrichs type numerical Hamiltonian

$$\hat{H}(p_1, p_2, q_1, q_2) = H\left(\frac{p_1 + p_2}{2}, \frac{q_1 + q_2}{2}\right) - \frac{1}{2}\alpha(p_1 - p_2) - \frac{1}{2}\beta(q_1 - q_2)$$

with

$$\alpha = \max_{p \in D, q \in E} \left| \frac{\partial H(p, q)}{\partial p} \right|.$$

With  $D = [\min(p_1, p_2), \max(p_1, p_2)]|_{\Omega}$  and  $E = [\min(q_1, q_2), \max(q_1, q_2)]|_{\Omega}$  we call it the global Lax–Friedrichs scheme. If  $D$  and  $E$  are rather local domain, in a word,  $D = [\min(p_1, p_2), \max(p_1, p_2)]|_K$  and  $E = [\min(q_1, q_2), \max(q_1, q_2)]|_K$  we call it the local Lax–Friedrichs scheme. Note similar fashion is applied to coefficient  $\beta$

$$\beta = \max_{p \in D, q \in E} \left| \frac{\partial H(p, q)}{\partial q} \right|.$$

### 4. Numerical examples

In this section we provide a series of numerical examples to illustrate the accuracy and the capacity of the LDG method for solving H–J equations. For time discretization explicit third order Runge–Kutta method [23,22] is used. We obtain optimal order of accuracy with piecewise  $p^k$  polynomial approximations and capture the viscosity (entropy) solution for both convex and noneconvex Hamiltonian. For two-dimensional examples, we use rectangular meshes in our numerical simulations.

#### Example 4.1. Variable coefficient linear Hamiltonian

$$\phi_t + \sin(x)\phi_x = 0, \quad 0 \leq x \leq 2\pi \tag{4.17}$$

**Table 4.1**  
1D variable coefficient linear problem (4.17).  $L^1$  and  $L^\infty$  errors at  $t = 1.0$ .  $p^k$  polynomial approximations with  $k = 0, 1, 2, 3$ .

$k$		$N = 40$		$N = 80$		$N = 160$		$N = 320$	
		Error	Order	Error	Order	Error	Order	Error	Order
0	$L^1$	2.47e–01		1.28e–01	0.95	6.52e–02	0.97	3.29e–02	0.99
	$L^\infty$	1.93e–01		9.80e–02	0.98	4.95e–02	0.98	2.48e–02	0.99
1	$L^1$	8.95e–03		2.28e–03	1.97	5.79e–04	1.98	1.46e–04	1.99
	$L^\infty$	1.63e–02		4.44e–03	1.87	1.15e–03	1.95	2.92e–04	1.98
2	$L^1$	3.63e–04		4.52e–05	3.00	5.67e–06	2.99	7.12e–07	2.99
	$L^\infty$	5.87e–04		9.10e–05	2.70	1.31e–05	2.80	1.85e–06	2.83
3	$L^1$	1.43e–05		9.14e–07	3.97	5.79e–08	3.98	3.66e–09	3.98
	$L^\infty$	2.74e–05		1.86e–06	3.88	1.24e–07	3.90	7.95e–09	3.97

with initial condition  $\phi(x, 0) = \sin(x)$  and periodic boundary condition. The exact solution is given as

$$\phi(x, t) = \sin\left(2 \tan^{-1}\left(e^{-t} \tan\left(\frac{x}{2}\right)\right)\right).$$

As discussed in Section 2, for variable coefficient linear problem (4.17) our LDG method (2.11) is not exactly the same as the standard DG method. We use this example to demonstrate that the same optimal order of accuracy can be obtained as the standard DG method for variable coefficient conservation laws. We compute the solution up to  $t = 1$  and check the  $L^1$  and  $L^\infty$  errors with refined mesh,  $(k + 1)$ th order of accuracy is obtained with  $p^k$  polynomial approximations. Results are listed in Table 4.1.

**Example 4.2.** Discontinuous variable coefficient linear Hamiltonian

$$\phi_t + \text{sign}(\cos(x))\phi_x = 0, \quad 0 \leq x \leq 2\pi \tag{4.18}$$

with initial  $\phi(x, 0) = \sin(x)$  and periodic boundary condition.

We take this example from [2], and use it to compare with the DG method in [2]. Due to the discontinuous variable coefficient profile, there will be a shock forming in  $\phi_x$  at  $x = \pi/2$  and a rarefaction wave forming at  $x = 3\pi/2$ . Fig. 4.1 lists our scheme simulations at time  $t = 1$  with piecewise constant up to piecewise cubic polynomial approximations. Note our scheme does not need entropy corrections to guarantee its convergence to the viscosity solution. On the other hand, we do need limiters (e.g. [21]) for higher order  $p^k (k \geq 2)$  polynomial approximations.

**Example 4.3.** Linear Hamiltonian with kink solutions

$$\phi_t + \phi_x = 0, \quad -1 \leq x < 1 \tag{4.19}$$

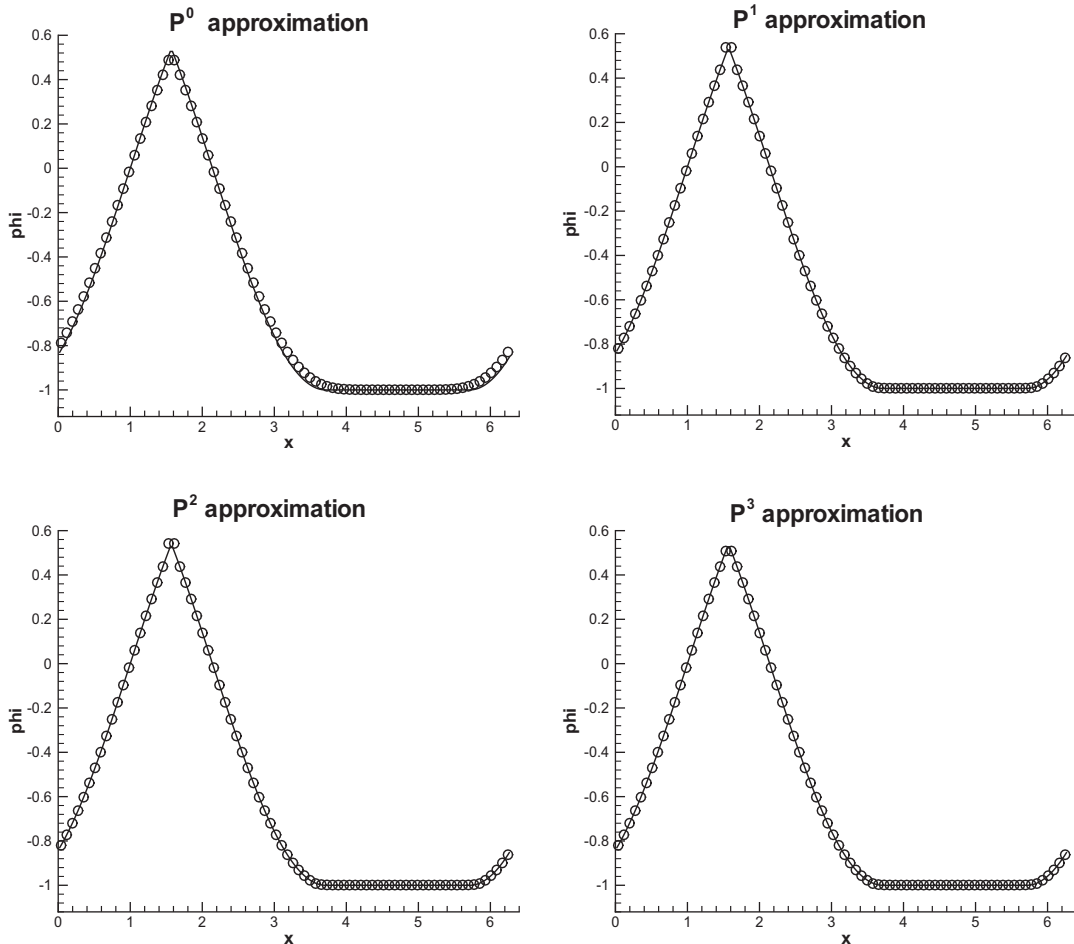


Fig. 4.1. Solid line is the exact solution. Symbol circle is the LDG approximation with mesh  $N = 80$ .

with initial  $\phi(x, 0) = g(x - 0.5)$  and periodic boundary condition, here

$$g(x) = -\left(\frac{\sqrt{3}}{2} + \frac{9}{2} + \frac{2\pi}{3}\right)(x + 1) + \begin{cases} 2 \cos\left(\frac{3\pi x^2}{2}\right) - \sqrt{3}, & -1 \leq x < -\frac{1}{3}; \\ \frac{3}{2} + \cos(2\pi x), & -\frac{1}{3} \leq x < 0; \\ \frac{15}{2} - 3 \cos(2\pi x), & 0 \leq x < \frac{1}{3}; \\ \frac{28 + 4\pi + \cos(3\pi x)}{3} + 6\pi x(x - 1), & \frac{1}{3} \leq x < 1. \end{cases}$$

We take the example from [15], and use it to test the ability of our scheme to catch the kinks after a long term run. We compute the LDG numerical solutions with piecewise linear and quadratic approximations up to  $t = 32$  (16 periods), see Fig. 4.2. We can observe better resolution with high order approximations, see the bottom two in Fig. 4.2 for  $p^2$  quadratic approximations. Compared to finite difference ENO/WENO schemes in [15,26], the DG method can better resolve corners with discontinuous derivatives even after a long term run (16 periods when  $t = 32$ ). This 1D example confirms the fact that DG method is better than finite difference WENO schemes when applied to level set equations for those volume reservation problems, see Example 4.2 in [19] with DG method and Example 3.1 in [13] with WENO5 scheme.

**Example 4.4.** Nonlinear convex Hamiltonian (1D Burgers equation)

$$\phi_t + \frac{(\phi_x + 1)^2}{2} = 0, \quad x \in [-1, 1] \tag{4.20}$$

with  $\phi(x, 0) = -\cos(\pi x)$  and periodic boundary condition.

The solution is smooth till the discontinuous derivative develops at  $t = \frac{1.0}{\pi^2}$ . We compute the  $L^1$  and  $L^\infty$  errors at  $t = \frac{0.5}{\pi^2}$  and  $t = \frac{3.5}{\pi^2}$ , before and after the singularity develops, and list the errors and orders in Tables 4.2 and 4.3. For  $t = \frac{3.5}{\pi^2}$ , the errors are computed away from the singularity with distance 0.15. Here we use the global Lax-Friedrichs scheme for the numerical

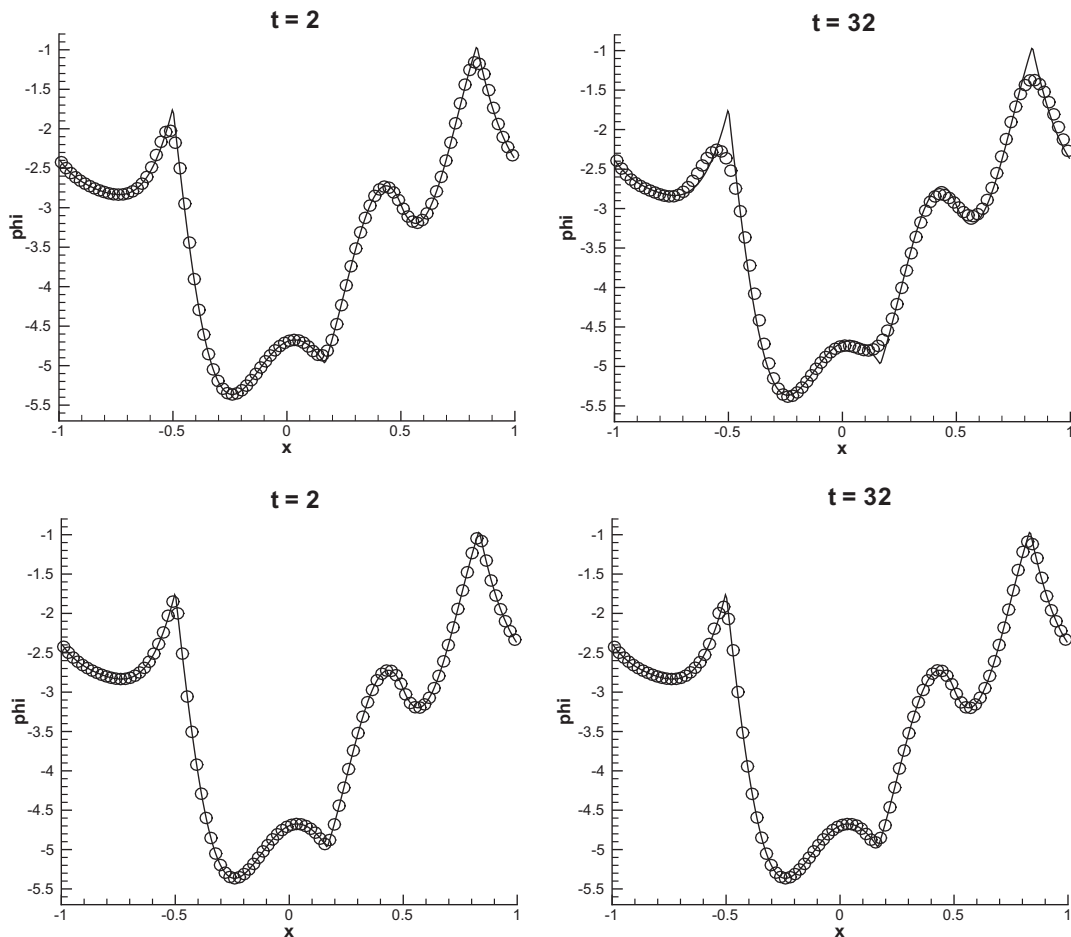


**Fig. 4.2.** Solid line is the exact solution. Symbol circle is LDG approximation with mesh  $N = 96$ . Top: linear approximation. Bottom: quadratic approximation.

**Table 4.2**

1D Burgers equation.  $L^1$  and  $L^\infty$  errors.  $p^k$  approximations with  $k = 0, 1, 2, 3$  at  $t = 0.5/\pi^2$ .

$k$		$N = 20$	$N = 40$		$N = 80$		$N = 160$	
		Error	Error	Order	Error	Order	Error	Order
0	$L^1$	1.35e-01	6.92e-02	0.96	3.51e-02	0.98	1.77e-02	0.99
	$L^\infty$	1.73e-01	9.08e-02	0.92	4.67e-02	0.96	2.36e-02	0.98
1	$L^1$	6.56e-03	1.75e-03	1.91	4.31e-04	2.02	1.07e-04	2.00
	$L^\infty$	1.34e-02	4.55e-03	1.56	1.12e-03	2.02	2.73e-04	2.03
2	$L^1$	2.26e-04	2.86e-05	2.98	3.57e-06	3.00	4.45e-07	3.00
	$L^\infty$	1.25e-03	1.88e-04	2.73	2.41e-05	2.96	2.93e-06	3.05
3	$L^1$	9.57e-05	7.98e-06	3.58	6.21e-07	3.68	4.33e-08	3.84
	$L^\infty$	2.35e-04	2.21e-05	3.41	1.75e-06	3.66	1.77e-07	3.30

**Table 4.3**

1D Burgers equations.  $L^1$  and  $L^\infty$  errors.  $p^k$  approximations with  $k = 0, 1, 2, 3$  at  $t = 3.5/\pi^2$ .

$k$		$N = 20$	$N = 40$		$N = 80$		$N = 160$	
		Error	Error	Order	Error	Order	Error	Order
0	$L^1$	1.80e-01	8.29e-02	1.11	3.98e-02	1.06	1.95e-02	1.02
	$L^\infty$	2.63e-01	1.37e-01	0.94	6.95e-02	0.98	3.48e-02	1.00
1	$L^1$	7.89e-03	1.30e-03	2.60	2.25e-04	2.52	4.17e-05	2.43
	$L^\infty$	3.93e-02	9.69e-03	2.02	2.32e-03	2.06	4.84e-04	2.26
2	$L^1$	7.15e-05	5.86e-06	3.60	6.78e-07	3.11	8.32e-08	3.02
	$L^\infty$	6.59e-04	1.15e-05	5.83	1.31e-06	3.13	1.60e-07	3.03
3	$L^1$	4.54e-06	3.09e-07	3.87	1.76e-08	4.13	9.31e-10	4.24
	$L^\infty$	1.07e-05	6.80e-07	3.97	4.20e-08	4.01	2.55e-09	4.04

Hamiltonian and roughly  $(k + 1)$ th order of accuracy is obtained with  $p^k$  polynomial approximations. In Fig. 4.3, we show the LDG approximation at  $t = \frac{3.5}{\pi^2}$  with  $p^1$  and  $p^2$  polynomials. The corner is clearly resolved for both piecewise linear and quadratic approximations.

Another example is the Burgers equation with none smooth initial condition in  $[0, 2\pi]$

$$\phi(x, 0) = \begin{cases} \pi - x, & x < \pi; \\ x - \pi, & x \geq \pi. \end{cases}$$

It is designed in [2] to check the convergence of the numerical solution to the entropy solution. In Fig. 4.4 we plot the LDG numerical solution with piecewise linear and quadratic approximations, clearly the LDG solution opens up and converges to the entropy solution.

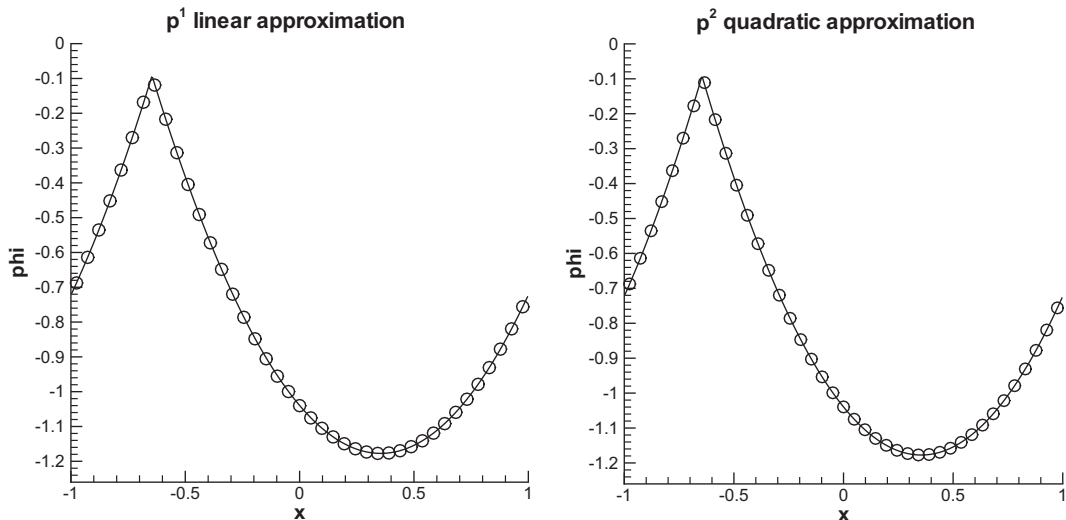


**Fig. 4.3.** 1D Burgers equation at  $t = \frac{3.5}{\pi^2}$  with mesh  $N = 41$ . Solid line is the exact solution and symbol circle are the  $p^1$  and  $p^2$  polynomial approximations.

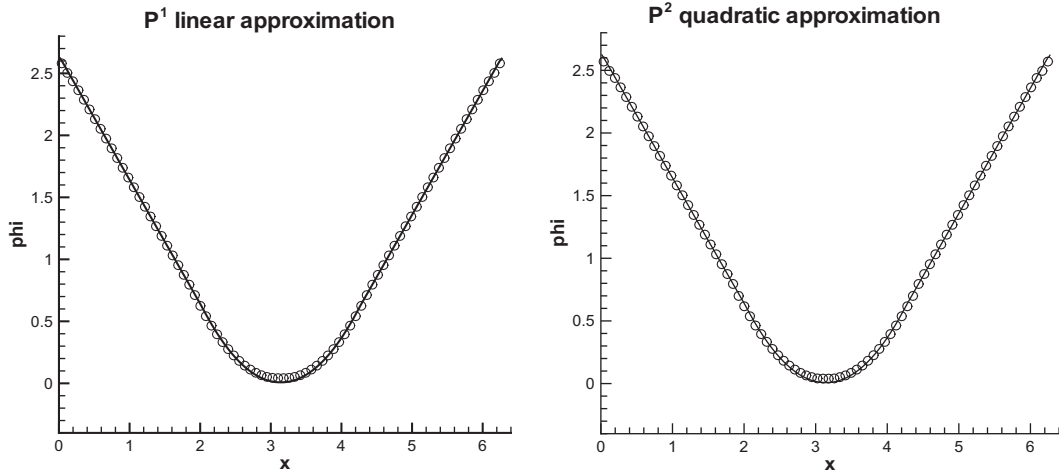


Fig. 4.4. Solid line is the exact solution and symbol circle is  $p^1$  and  $p^2$  polynomial approximations at  $t = 1$  with  $N = 80$ .

**Example 4.5.** 1D nonconvex Hamiltonian

$$\phi_t - \cos(\phi_x + 1) = 0, \quad x \in [-1, 1] \tag{4.21}$$

with  $\phi(x, 0) = -\cos(\pi x)$  and periodic boundary condition.

Similar to the previous example, discontinuous derivative appears at  $t = \frac{1.0}{\pi^2}$ . We compute the  $L^1$  and  $L^\infty$  errors and obtain  $(k + 1)$ th order of accuracy for  $t = \frac{0.5}{\pi^2}$  and  $t = \frac{1.5}{\pi^2}$ , before and after discontinuous derivatives developed, see Tables 4.4 and 4.5. In Fig. 4.5 we show the LDG approximations at  $t = \frac{1.5}{\pi^2}$  and kinks are clearly resolved.

**Example 4.6.** 1D Riemann problem with nonconvex Hamiltonian

**Table 4.4**

1D nonconvex problem (4.21).  $L^1$  and  $L^\infty$  errors.  $p^k$  polynomial approximations with  $k = 0, 1, 2, 3$  at  $t = 0.5/\pi^2$ .

$k$		$N = 20$		$N = 40$		$N = 80$		$N = 160$	
		Error	Order	Error	Order	Error	Order	Error	Order
0	$L^1$	1.03e-01	1.00	5.13e-02	1.00	2.56e-02	1.00	1.28e-02	1.00
	$L^\infty$	1.44e-01	1.00	7.21e-02	1.00	3.61e-02	1.00	1.80e-02	1.00
1	$L^1$	6.01e-03	2.01	1.49e-03	2.01	3.69e-04	2.01	9.22e-05	1.99
	$L^\infty$	2.11e-03	1.75	6.25e-04	1.75	1.44e-04	2.12	3.70e-05	1.96
2	$L^1$	2.90e-04	3.13	3.31e-05	3.13	4.19e-06	2.98	5.19e-07	3.01
	$L^\infty$	2.22e-04	2.61	3.63e-05	2.61	5.66e-06	2.68	7.57e-07	2.90
3	$L^1$	1.22e-05	3.36	1.18e-06	3.36	7.59e-08	3.96	4.61e-09	4.04
	$L^\infty$	8.39e-05	2.80	1.20e-05	2.80	1.35e-06	3.15	9.05e-08	3.91

**Table 4.5**

1D nonconvex problem (4.21).  $L^1$  and  $L^\infty$  errors.  $p^k$  polynomial approximations with  $k = 0, 1, 2, 3$  at  $t = 1.5/\pi^2$ . Errors are computed in interval  $[-0.25, 0]$  in which the solution is smooth.

$k$		$N = 20$		$N = 40$		$N = 80$		$N = 160$	
		Error	Order	Error	Order	Error	Order	Error	Order
0	$L^1$	5.02e-02	1.10	2.33e-02	1.10	1.17e-02	0.99	5.84e-03	1.00
	$L^\infty$	1.72e-01	0.98	8.70e-02	0.98	4.36e-02	0.99	2.17e-02	1.00
1	$L^1$	3.18e-03	2.14	7.20e-04	2.14	1.75e-04	2.04	4.31e-05	2.02
	$L^\infty$	1.42e-02	2.22	3.05e-03	2.22	7.53e-04	2.01	1.80e-04	2.02
2	$L^1$	7.26e-05	3.22	7.75e-06	3.22	9.47e-07	3.03	1.16e-07	3.01
	$L^\infty$	7.84e-04	3.04	9.49e-05	3.04	1.25e-05	2.92	1.55e-06	3.01
3	$L^1$	5.50e-06	4.35	2.68e-07	4.35	1.70e-08	3.98	1.05e-09	4.01
	$L^\infty$	4.57e-05	3.23	4.86e-06	3.23	3.26e-07	3.90	2.00e-08	4.02

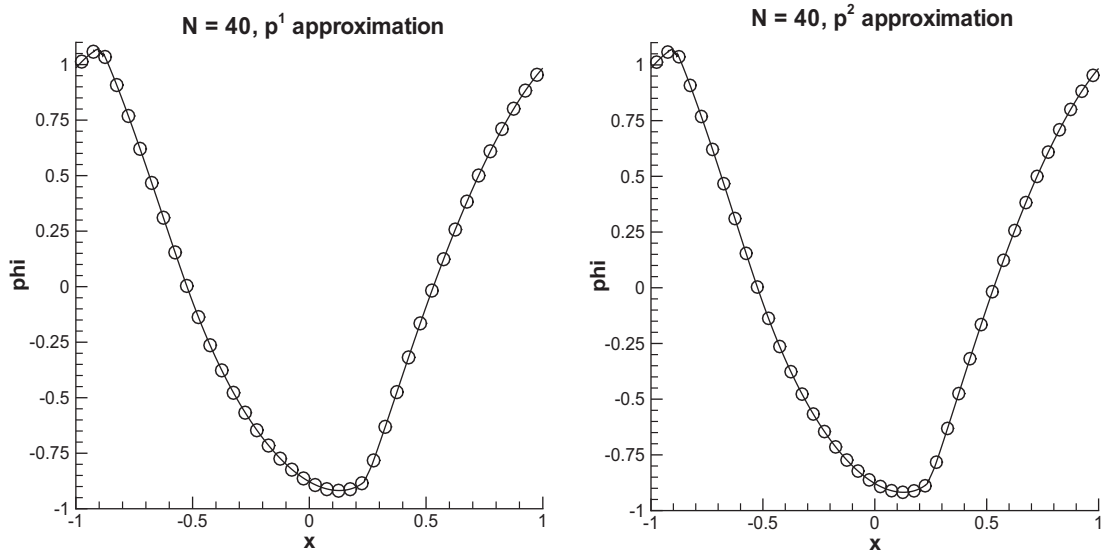


Fig. 4.5. 1D noneconvex Hamiltonian with piecewise linear and quadratic approximation at  $t = 1.5/\pi^2$ .

$$\phi_t + \frac{1}{4}(\phi_x^2 - 1)(\phi_x^2 - 4) = 0, \quad x \in [-1, 1] \tag{4.22}$$

with initial condition as  $\phi(x, 0) = -2|x|$ .

This is a benchmark problem to test a numerical scheme’s capability to capture the entropy (viscosity) solution. The corresponding conservation law for  $\phi_x$  have two shocks propagating to the left and the right connected in between with a rarefaction wave. With piecewise constant approximation our LDG scheme is monotone, and converges to the entropy solution. With piecewise linear or higher order approximations, limiter is needed for the convergence to the entropy solution. For this example and the 2D Riemann problem we use the TVB slope limiter as in [21]. Numerical results at  $t = 1$  with 81 elements, using the local Lax–Friedrichs flux, is shown in Fig. 4.6. Exact solutions are used as the given boundary condition.

**Example 4.7. 2D Burgers equation**

$$\phi_t + \frac{(\phi_x + \phi_y + 1)^2}{2} = 0, \quad x \in \Omega = [-2, 2] \times [-2, 2] \tag{4.23}$$

with initial condition  $\phi(x, y, 0) = -\cos\left(\frac{\pi(x+y)}{2}\right)$  and periodic boundary conditions.

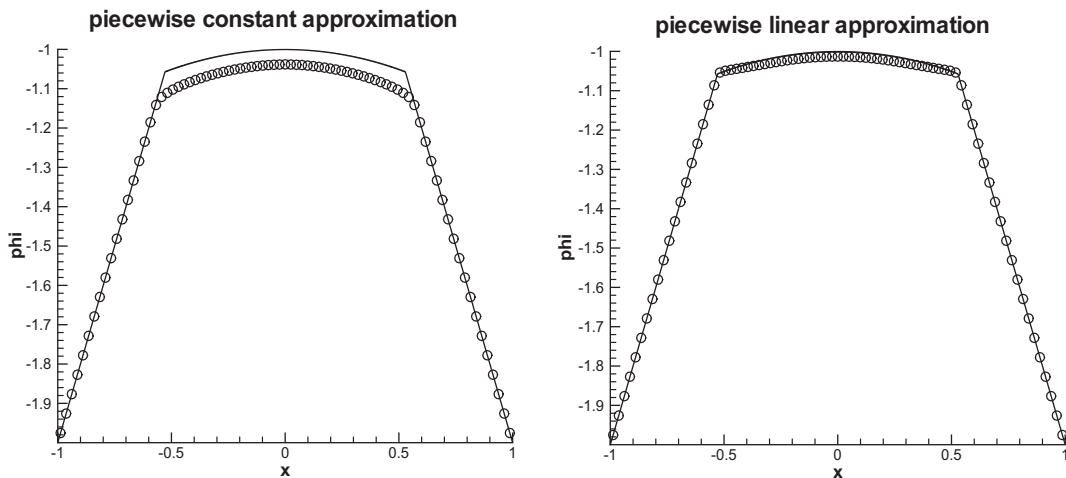


Fig. 4.6. 1D Riemann problem with none convex Hamiltonian (4.22) mesh  $N = 81$  at  $t = 1$ .

We use local Lax–Friedrichs numerical Hamiltonian in the computations. At  $t = \frac{0.5}{\pi^2}$ , the solution is still smooth. We compute the  $L^1$  and  $L^\infty$  errors with  $p^k$  ( $k = 0, 1, 2$ ) polynomial approximations, and list the errors and order of accuracy in Table 4.6. At  $t = \frac{1.5}{\pi^2}$  the discontinuous derivative has developed, the result of LDG solution is shown in Fig. 4.7.

**Example 4.8.** 2D problem with nonconvex Hamiltonian

$$\phi_t - \cos(\phi_x + \phi_y + 1) = 0, \quad (x, y) \in \Omega = [-2, 2] \times [-2, 2] \tag{4.24}$$

with initial condition  $\phi(x, y, 0) = -\cos\left(\frac{\pi(x+y)}{2}\right)$  and periodic boundary conditions.

Similar to the previous case, the solution develops discontinuous derivatives at  $t = \frac{1.0}{\pi^2}$ . We check the LDG errors and order of convergence at  $t = \frac{0.5}{\pi^2}$ , and we obtain  $(k + 1)$ th order of accuracy, see Table 4.7. Fig. 4.8 shows the LDG numerical solution approximation at  $t = \frac{1.5}{\pi^2}$  where corners have developed.

**Example 4.9.** 2D Riemann problem

$$\phi_t + \sin(\phi_x + \phi_y) = 0, \quad x \in \Omega = [-1, 1] \times [-1, 1] \tag{4.25}$$

with initial condition  $\phi(x, y, 0) = \pi(|y| - |x|)$ . With piecewise constant approximations LDG scheme degenerates to the monotone scheme, so it converges to the viscosity solution. With piecewise linear or higher order polynomial approximations, we

**Table 4.6**  
2D Burgers equation (4.23).  $L^1$  and  $L^\infty$  errors at  $t = \frac{0.5}{\pi^2}$ ,  $p^k$  polynomial approximation with  $k = 0, 1, 2$ .

$k$		$N = 10$		$N = 20$		$N = 40$		$N = 80$	
		Error	Order	Error	Order	Error	Order	Error	Order
0	$L^1$	2.01e-01	0.99	1.03e-01	0.99	5.13e-02	1.00	2.56e-02	1.00
	$L^\infty$	2.93e-01	1.02	1.44e-01	1.02	7.21e-02	1.00	3.61e-02	1.00
1	$L^1$	2.43e-02	2.00	6.01e-03	2.00	1.49e-03	2.01	3.69e-04	2.01
	$L^\infty$	9.60e-03	1.70	2.88e-03	1.70	6.25e-04	1.75	1.44e-04	2.12
2	$L^1$	2.33e-03	3.01	2.90e-04	3.01	3.31e-05	3.13	4.19e-06	2.98
	$L^\infty$	1.65e-03	2.56	2.22e-04	2.56	3.63e-05	2.61	5.66e-06	2.68

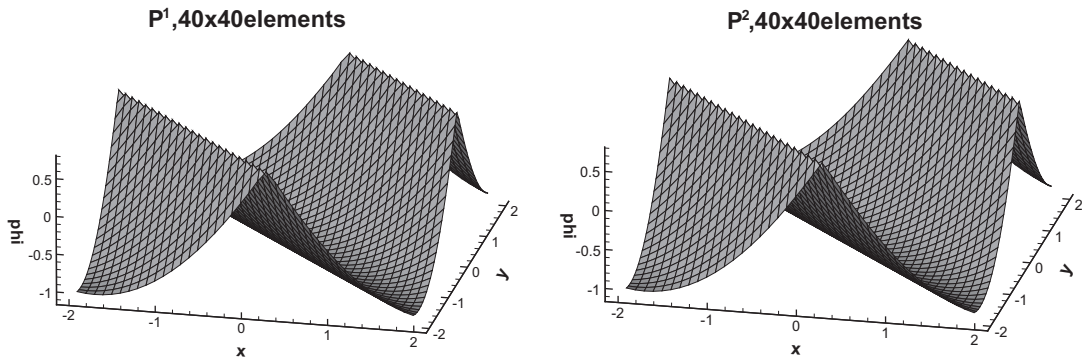


**Fig. 4.7.** 2D Burgers equation (4.23) at  $t = 1.5/\pi^2$  where corner has developed.  $p^1$  and  $p^2$  polynomial approximations with mesh  $N = 40 \times 40$ .

**Table 4.7**  
2D problem with nonconvex Hamiltonian (4.24).  $L^1$  and  $L^\infty$  errors at  $t = \frac{0.5}{\pi^2}$  with  $k = 0, 1, 2$ .

$k$		$N = 10$		$N = 20$		$N = 40$		$N = 80$	
		Error	Order	Error	Order	Error	Order	Error	Order
0	$L^1$	1.35e-01	0.97	6.90e-02	0.97	3.47e-02	0.99	1.74e-02	1.00
	$L^\infty$	6.07e-01	0.99	3.05e-01	0.99	1.51e-01	1.01	7.31e-02	1.05
1	$L^1$	5.34e-02	1.78	1.56e-02	1.78	4.03e-03	1.95	9.73e-04	2.05
	$L^\infty$	1.02e-01	1.84	2.85e-02	1.84	7.80e-03	1.87	2.10e-03	1.90
2	$L^1$	7.83e-03	2.50	1.38e-03	2.50	2.12e-04	2.71	3.08e-05	2.78
	$L^\infty$	4.48e-02	2.35	8.79e-03	2.35	1.52e-03	2.53	2.55e-04	2.58

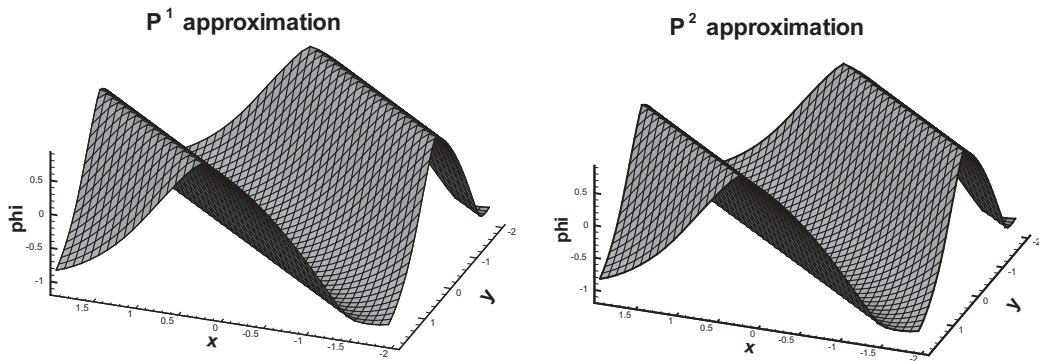


Fig. 4.8. 2D equation with non-convex Hamiltonian (4.24).  $t = \frac{1.5}{\pi^2}$ ,  $p^1$  and  $p^2$  polynomial approximations with mesh  $N = 40 \times 40$ .

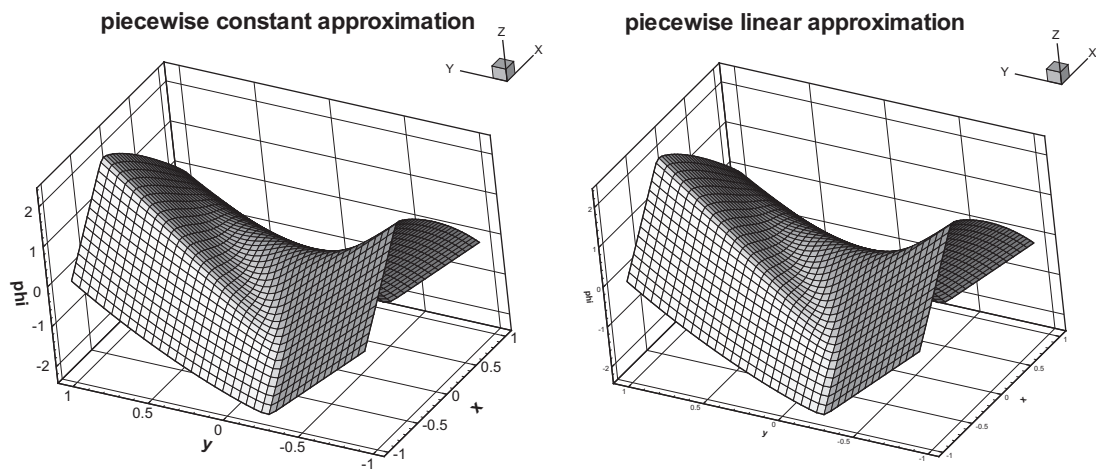


Fig. 4.9. 2D Riemann problem (4.25) at  $t = 1$ , piecewise constant and linear polynomial approximation with mesh  $N = 40 \times 40$ .

need limiters in this example to have its convergence to the viscosity solution. LDG approximation with mesh  $N = 40 \times 40$  at  $t = 1$  is listed in Fig. 4.9.

## Acknowledgments

The authors thank the anonymous referees for their valuable suggestions and comments that result in the improvements of the paper.

## References

- [1] F. Bassi, S. Rebay, A high-order accurate discontinuous finite element method for the numerical solution of the compressible Navier–Stokes equations, *J. Comput. Phys.* 131 (2) (1997) 267–279.
- [2] Y. Cheng, C.-W. Shu, A discontinuous Galerkin finite element method for directly solving the Hamilton–Jacobi equations, *J. Comput. Phys.* 223 (1) (2007) 398–415.
- [3] B. Cockburn, S. Hou, C.-W. Shu, The Runge–Kutta local projection discontinuous Galerkin finite element method for conservation laws. IV. The multidimensional case, *Math. Comput.* 54 (190) (1990) 545–581.
- [4] B. Cockburn, G.E. Karniadakis, C.-W. Shu, The development of discontinuous Galerkin methods, in: *Discontinuous Galerkin Methods* (Newport, RI, 1999), Lecture Notes in Computational Science and Engineering, vol. 11, Springer, Berlin, 2000, pp. 3–50.
- [5] B. Cockburn, S.Y. Lin, C.-W. Shu, TVB Runge–Kutta local projection discontinuous Galerkin finite element method for conservation laws. III. One-dimensional systems, *J. Comput. Phys.* 84 (1) (1989) 90–113.
- [6] B. Cockburn, C.-W. Shu, TVB Runge–Kutta local projection discontinuous Galerkin finite element method for conservation laws. II. General framework, *Math. Comput.* 52 (186) (1989) 411–435.
- [7] B. Cockburn, C.-W. Shu, The Runge–Kutta local projection  $P^1$ -discontinuous-Galerkin finite element method for scalar conservation laws, *RAIRO Modél. Math. Numér.* 25 (3) (1991) 337–361.
- [8] B. Cockburn, C.-W. Shu, The local discontinuous Galerkin method for time-dependent convection–diffusion systems, *SIAM J. Numer. Anal.* 35 (6) (1998) 2440–2463 (electronic).

- [9] B. Cockburn, C.-W. Shu, The Runge–Kutta discontinuous Galerkin method for conservation laws. V. Multidimensional systems, *J. Comput. Phys.* 141 (2) (1998) 199–224.
- [10] B. Cockburn, C.-W. Shu, Runge–Kutta discontinuous Galerkin methods for convection-dominated problems, *J. Sci. Comput.* 16 (3) (2001) 173–261.
- [11] M.G. Crandall, P.-L. Lions, Viscosity solutions of Hamilton–Jacobi equations, *Trans. Am. Math. Soc.* 277 (1) (1983) 1–42.
- [12] M.G. Crandall, P.-L. Lions, Two approximations of solutions of Hamilton–Jacobi equations, *Math. Comput.* 43 (167) (1984) 1–19.
- [13] D. Enright, R. Fedkiw, J. Ferziger, I. Mitchell, A hybrid particle level set method for improved interface capturing, *J. Comput. Phys.* 183 (1) (2002) 83–116.
- [14] C. Hu, C.-W. Shu, A discontinuous Galerkin finite element method for Hamilton–Jacobi equations, *SIAM J. Sci. Comput.* 21 (2) (1999) 666–690 (electronic).
- [15] G.-S. Jiang, D. Peng, Weighted ENO schemes for Hamilton–Jacobi equations, *SIAM J. Sci. Comput.* 21 (6) (2000) 2126–2143 (electronic).
- [16] D. Levy, C.-W. Shu, J. Yan, Local discontinuous Galerkin methods for nonlinear dispersive equations, *J. Comput. Phys.* 196 (2) (2004) 751–772.
- [17] F. Li, S. Yakovlev, A central discontinuous Galerkin method for Hamilton–Jacobi equations, *J. Sci. Comput.* doi:10.1007/s10915-009-9340-y.
- [18] H. Liu, J. Yan, A local discontinuous Galerkin method for the Korteweg–de Vries equation with boundary effect, *J. Comput. Phys.* 215 (1) (2006) 197–218.
- [19] E. Marchandise, J.-F. Remacle, N. Chevaugeon, A quadrature-free discontinuous Galerkin method for the level set equation, *J. Comput. Phys.* 212 (1) (2006) 338–357.
- [20] S. Osher, J.A. Sethian, Fronts propagating with curvature-dependent speed: algorithms based on Hamilton–Jacobi formulations, *J. Comput. Phys.* 79 (1) (1988) 12–49.
- [21] S. Osher, C.-W. Shu, High-order essentially nonoscillatory schemes for Hamilton–Jacobi equations, *SIAM J. Numer. Anal.* 28 (4) (1991) 907–922.
- [22] C.-W. Shu, S. Osher, Efficient implementation of essentially nonoscillatory shock-capturing schemes, *J. Comput. Phys.* 77 (2) (1988) 439–471.
- [23] C.-W. Shu, S. Osher, Efficient implementation of essentially nonoscillatory shock-capturing schemes. II, *J. Comput. Phys.* 83 (1) (1989) 32–78.
- [24] Y. Xu, C.-W. Shu, Local discontinuous Galerkin methods for nonlinear Schrödinger equations, *J. Comput. Phys.* 205 (1) (2005) 72–97.
- [25] J. Yan, C.-W. Shu, A local discontinuous Galerkin method for KdV type equations, *SIAM J. Numer. Anal.* 40 (2) (2002) 769–791 (electronic).
- [26] Y.-T. Zhang, C.-W. Shu, High-order WENO schemes for Hamilton–Jacobi equations on triangular meshes, *SIAM J. Sci. Comput.* 24 (3) (2002) 1005–1030 (electronic).